Biochimie 95 (2013) 1939–1948

Contents lists available at SciVerse ScienceDirect

Biochimie

journal homepage: www.elsevier.com/locate/biochi

Research paper

The attack of the phytopathogens and the trumpet solo: Identification of a novel plant antifungal peptide with distinct fold and disulfide bond pattern

Santi M. Mandal [a], William F. Porto [b], Prabuddha Dey [c], Mrinal K. Maiti [c], Ananta K. Ghosh [c], Octavio L. Franco [b,*]

[a] Central Research Facility, Indian Institute of Technology Kharagpur, Kharagpur 721302, India
[b] Centro de Análises Proteômicas e Bioquímicas, Pós-Graduação em Ciências Genômicas e Biotecnologia UCB, Brasília, DF, Brazil
[c] Department of Biotechnology, Indian Institute of Technology Kharagpur, Kharagpur 721302, India

ARTICLE INFO

Article history:
Received 5 April 2013
Accepted 28 June 2013
Available online 5 July 2013

Keywords:
αβ-Trumpet
Antifungal peptides
Pisum sativum
Plant defense
Lectin-like peptides
Molecular dynamics

ABSTRACT

Phytopathogens cause economic losses in agribusiness. Plant-derived compounds have been proposed to overcome this problem, including the antimicrobial peptides (AMPs). This paper reports the identification of Ps-AFP1, a novel AMP isolated from the *Pisum sativum* radicle. Ps-AFP1 was purified and evaluated against phytopathogenic fungi, showing clear effectiveness. *In silico* analyses were performed, suggesting an unusual fold and disulfide bond pattern. A novel fold and a novel AMP class were here proposed, the αβ-trumpet fold and αβ-trumpet peptides, respectively. The name αβ-trumpet was created due to the peptide's fold, which resembles the musical instrument. The Ps-AFP1 mechanism of action was also proposed. Microscopic analyses revealed that Ps-AFP1 could affect the fungus during the hyphal elongation from spore germination. Furthermore, confocal microscopy performed with Ps-AFP1 labeled with FITC shows that the peptide was localized at high concentration along the fungal cell surface. Due to low cellular disruption rates, it seems that the main target is the fungal cell wall. The binding thermogram and isothermal titration, molecular dynamics and docking analyses were also performed, showing that Ps-AFP1 could bind to chitin producing a stable complex. Data here reported provided novel structural–functional insights into the αβ-trumpet peptide fold.

1. Introduction

Phytopathogenic fungi may cause enormous problems in agribusiness, generating severe economic losses, since plants provide the main source of nutrition for these pathogens [1]. However, several plant-derived compounds have been reported as defense mechanisms, activated upon pathogen attack [2]. Among such mechanisms, the antimicrobial peptides (AMPs) have been described as being able to kill or slow the growth of infecting microorganisms and help to develop plant adaptive immunity [3]. In this field, AMPs provide innate immunity by the rapid formation of a "first defense line" against phytopathogens.

Hundreds of different antimicrobial proteins and peptides encoded within the genomes of plants have been described [3–5], and plant seeds have been used as a target for identification of plant AMPs. Several plant AMPs have been isolated from plant seeds, such as Pg-AMP1 [6], Cr-ACP1 [7], Cp-AMP [8] and Cp-thionin [9]. The AMPs can be classified in two major groups, according to the presence or absence of disulfide bridges [10]. The disulfide-free peptides are composed mainly of α-helical and unstructured AMPs; while the cysteine-stabilized AMPs can have a number of different folds. The plant cysteine-stabilized AMPs are classified according to their folds and disulfide patterns, so that the discovery of a novel fold could lead to a re- classification or to the creation of a novel AMP class [2,11,12]. In plants, there are few examples of plant disulfide-free AMPs [6,7,13–15], with most plant AMPs stabilized by disulfide bonds [2,4]. The main plant cysteine-stabilized AMP classes are thionins [16,17], defensins [18,19], cyclotides [20,21], hevein-like peptides [5,22], helical hairpins [23,24] and snakins [25–27]. Indeed, a more accurate classification could lead to a better understanding of structural–functional relations, despite the fact that the multifunctional character of AMPs [28] has made it difficult to acquire a complete understanding of their mechanisms of action.

* Corresponding author. Tel.: +55 6134487167.
E-mail addresses: ocfranco@gmail.com, ocfranco@pos.ucb.br (O.L. Franco).

0300-9084/$ – see front matter © 2013 Elsevier Masson SAS. All rights reserved.
http://dx.doi.org/10.1016/j.biochi.2013.06.027

Here, the identification of a novel small antimicrobial peptide with a distinct fold and disulfide bond pattern, Ps-AFP1, is reported. Ps-AFP1 was isolated from the *Pisum sativum* radicle, a very soft tissue, which grows downward in soil and survives on the fungal and bacterial population. Moreover, *in silico* analyses were performed, suggesting an unusual disulfide bond pattern and also an unusual fold. Therefore, the class of αβ-trumpet peptides is proposed here. The Ps-AFP1 mechanism of action was also proposed by using scanning electron and confocal microscopy analyses. Finally, molecular dynamics and docking analyses were also performed in order to better understand the structure–function relationship.

2. Results

2.1. Purification and sequencing of Ps-AFP1

In order to explore the radicle peptide content, an RP-HPLC-based separation strategy was used (Fig. 1(a)), yielding multiple fractions. After lyophilization, all fractions were challenged against fungi and one of them (star-marked in Fig. 1(a)) showed the highest efficiency. This fraction was submitted to rechromatography and after purification was named Ps-AFP1. Pure peptide (>90% after rechromatography, Fig. 1(b)) was obtained at a yield of ~0.18 mg from 100 g of radicle flour. The monoisotopic molecular mass of Ps-AFP1 was *m*/*z* 4198 Da (Fig. 1(c)). The presence of cysteine residues in Ps-AFP1 was confirmed by MALDI-MS analysis of reduced peptide after alkylation, which showed an addition of *m*/*z* 57 Da in each cysteine residue (data not shown). Firstly, the N-terminal sequence of Ps-AFP1 was determined as ^{1}RQLKS^{5}. In order to complete this sequence, a 5′-forward primer obtained from N-terminal sequence primers was constructed and a 3′-RACE-based poly (A) tail containing cDNA was used to amplify the corresponding Ps-AFP1gene sequence. The obtained cDNA sequence of Ps-AFP1 was "CGCCAGCTGAAAAGCAGCCGCCGCGGCGCGCTG GTGTGCGTGCGCCTGAAACTGTGCAGCGCGATTCTGAGCCGCGGCCT-GAGCTGCGGCATGTTTAGCTGCAACGCGCGCCGC" and the corresponding amino acid sequence was ^{1}RQLKSSRRGALVCVRLKLC SAILSRGLSCGMFSCNARR^{38} (Fig. S1).

Table 1
Antifungal activities of Ps-AFP1.

Fungus	EC_{50} (μM)
Aspergillus niger	15.62
Aspergillus terreus	7.81
Fusarium solani	7.81
Fusarium oxysporum	3.91
Pythium sp.	15.62
Colletotrichum gloeosporioides	7.81
Candida albicans	3.91
Glomerella sp.	7.81

2.2. Antifungal activity of Ps-AFP1

The antifungal activity was evaluated against several soil-borne plant pathogens. Ps-AFP1 exhibited different antifungal activities against most of the pathogens used (Table 1). These phytopathogenic fungi mostly cause damping-off diseases of seeds, seedlings and roots. The EC_{50} values were ranged at 0.975–500 μM, where *Fusarium oxysporum* and *Candida albicans* were the most affected

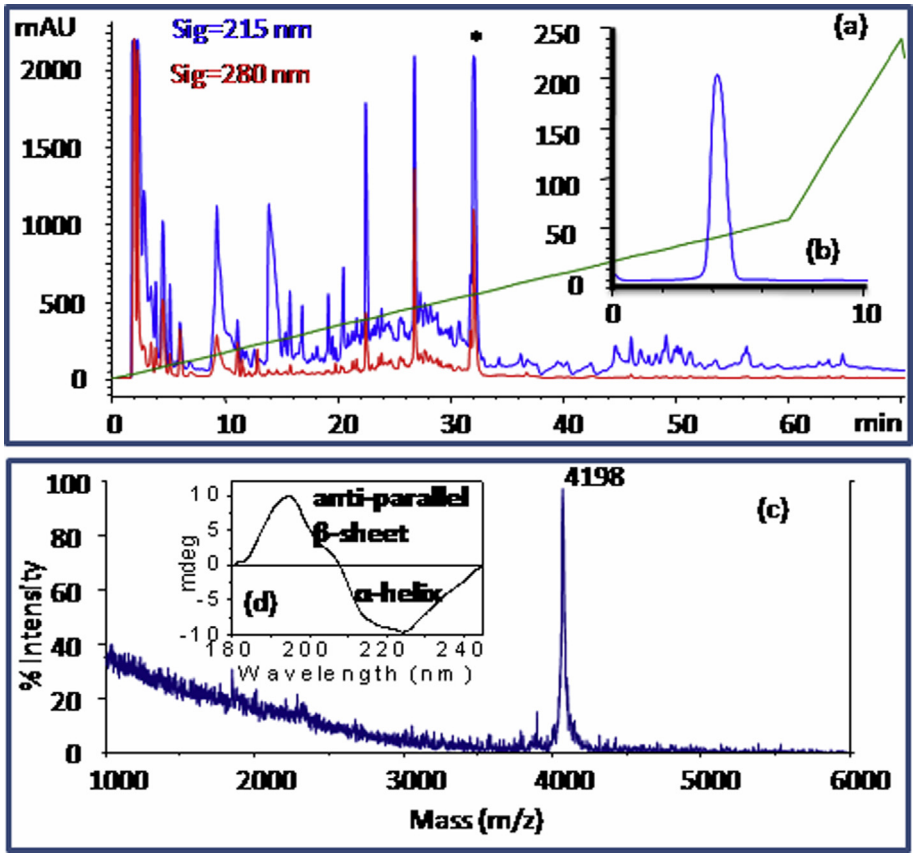

Fig. 1. Purification profile of Ps-AFP1 extracted from radicle of garden pea *Pisum sativum*. Reversed-phase HPLC chromatogram profile of acetic acid extract (a); diagonal line indicates the gradient of solvent B; rechromatogram profile of asterisk-indicated fraction (b, in inset); the mobile phase and other conditions are described in the text. MALDI TOF mass spectrum of asterisk-indicated antifungal active fraction (c), CD spectra of Ps-AFP1 in buffer solution (d).

species and *Aspergillus niger* and *Pythium* sp. were the least affected by Ps-AFP1. Moreover, in order to better understand the Ps-AFP1 killing kinetics, *C. albicans* and *Colletotrichum gloeosporioides* were challenged with different peptide concentrations. Data reported suggest that Ps-AFP1 inhibits fungal growth in a dose-dependent manner (Fig. S3).

2.3. Inhibition of spore germination

Spore germination of *Aspergillus solani* and *Fusarium solani* was remarkably (70%) inhibited by the presence of Ps-AFP1 with their corresponding EC_{50} values (8 μM). Spore germination inhibition was mostly influenced after 6 h incubation (data not shown). In this period, a phase contrast microscopic analysis was performed, revealing that Ps-AFP1 could directly affect fungal spore and further inhibit the hyphal elongation from the germinating spore (Fig. 2).

2.4. Confocal microscopy

The localization of FITC-labeled Ps-AFP1 on treated *Candida* cells was monitored by confocal microscopy. First it was checked and confirmed that FITC-conjugated Ps-AFP1 retained identical antifungal activity without conjugation and CFW does not altered the activity of FITC-conjugated Ps-AFP1 (data not shown). Confocal microscopic images revealed that Ps-AFP1 was localized on the cell surface and increased the Ps-AFP (green fluorescence) concentration on the surface as incubation time increased. After 10 min of incubation, Ps-AFP1 was found to be predominant along the cell surface, and a few granules were also localized in the center, indicating the entrance of Ps-AFP1 into the cytoplasm at very low concentrations (Fig. 3).

2.5. Circular dichroism analysis

The secondary structures of the peptides were investigated by using circular dichroism (CD) (Fig. 1(d)). The CD spectra revealed a negative peak at 215 nm, indicating the formation of β-sheets structure, and a wide shoulder near 223 nm, indicating α-helical conformation. The CD spectrum is characterized by a strong positive band between 195 and 198 nm, corresponding to the formation of antiparallel β-sheet structure.

2.6. Isothermal titration calorimeter analysis

The binding thermogram and isotherm for the N,N,N-triacetylchitotriose ($(GlcNAc)_3$) are shown in Fig. 4. The binding constant of Ps-AFP1 to $(GlcNAc)_3$ was determined to be $9.4 \pm 1.1 \times 10^3\ M^{-1}$. The moderate binding constant might be due to the use of only a single unit of $(GlcNAc)_3$. The interactions between $(GlcNAc)_3$ and Ps-AFP1 are enthalpically favored ($\Delta H = -1.689E4$), providing reaction negative enthalpy values at 25 °C (Fig. 4). The negative free energy of reaction values suggested that these binding interactions are all spontaneous reactions.

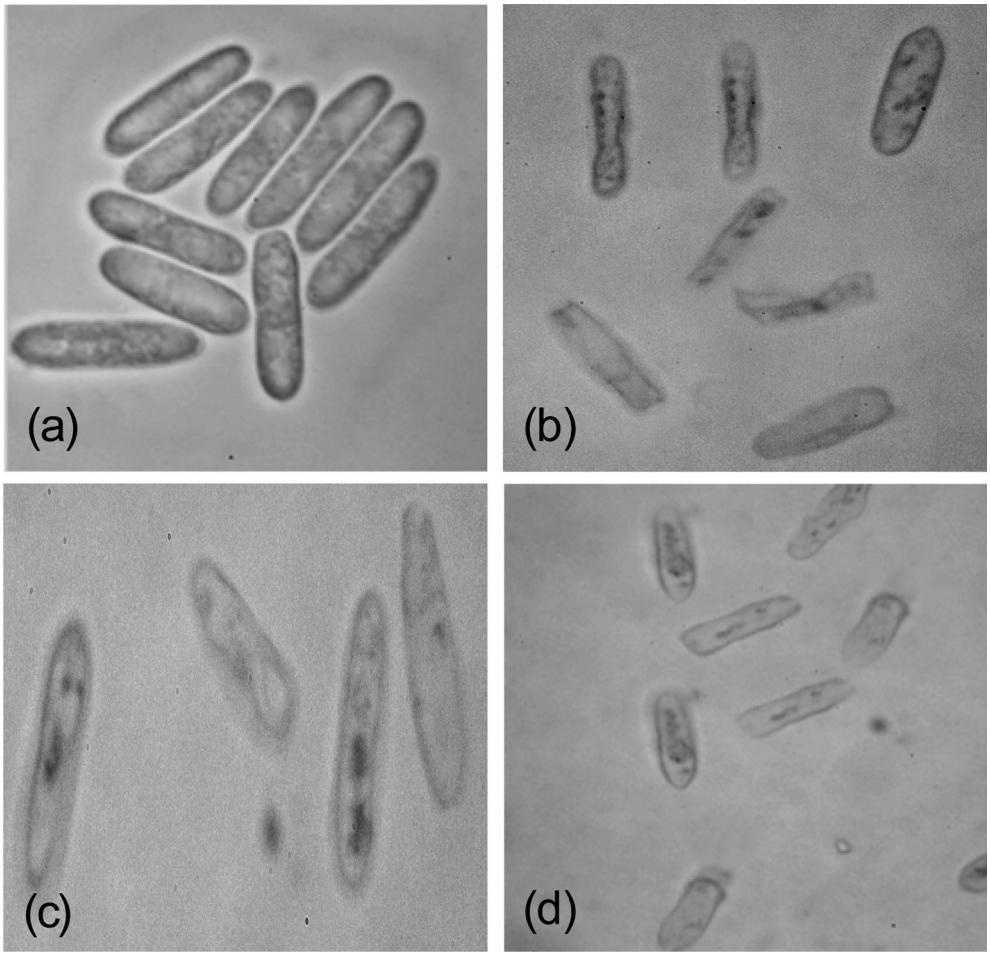

Fig. 2. Phase contrast microscopic images of spore germination inhibition by Ps-AFP1. Spores of *Glomerella* sp. were incubated with PBS (1×) for 2 h (a) and 6 h (c); simultaneously with Ps-AFP1 (8 μM) for 2 h (b) and 6 h (d). Images show that Ps-AFP1 has an adverse effect on spore germination. Images were captured at 1000× magnification.

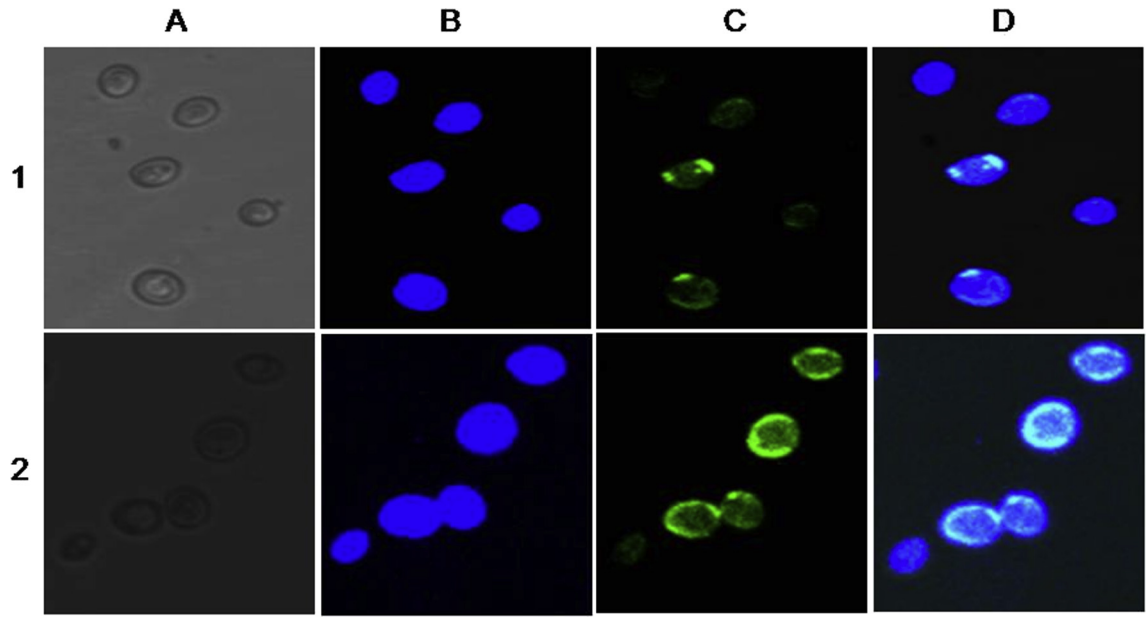

Fig. 3. Confocal microscopic images of *Candida* cells treated with Ps-AFP1. *Candida* cells were successively treated with CFW dye and FITC-conjugated Ps-AFP1, viewed in confocal microscope at 400× magnification. Cells were treated with FITC-conjugated Ps-AFP1 for 5 min (upper panel, 1) and for 10 min (lower panel, 2). Images were captured from the same field of interest in bright field (A), under 355 nm laser, showing blue color due to the excitation of AFW dye (B), under 488 nm laser showing green color due to the excitation of FITC dye (C) and merged view of both AFW and FITC-conjugated Ps-AFP1 showing light cyan color (D). Images revealed the localization of Ps-AFP1 mainly on the cell surface.

2.7. *In silico analyses*

Ps-AFP1 was predicted to be an antimicrobial by CS-AMPPred, with a score of 0.8042, indicating that its physicochemical and structural properties (charge, hydrophobicity, flexibility, α-helix and loop indexes) are similar to other cysteine-stabilized AMPs. However, no hits were returned by PSI-BLAST and InterPro Scan, nor in the search for similar structures deposited in PDB through LOMETS. Therefore, the QUARK *ab initio* server was used to predict the Ps-AFP1 tertiary structure, which was expected to be composed of an α-helix and an antiparallel β-sheet with two β-strands, being stabilized by two disulfide bridges formed between Cys^{13} and Cys^{19}; and Cys^{29} and Cys^{34} (Fig. 5). In the Ramachandran plot, 72.7% of the residues are in favored regions; and 24.2% are in additional allowed regions; and the overall G-Factor was −0.04. The *Z*-score on ProSA was −6.61. Since the scanning electron and the confocal microscopies indicated, respectively, a deleterious effect on the germinating spore and a high peptide concentration on the cell surface, the fungal cell wall was proposed as the main Ps-AFP1 target. Therefore, the docking with $(GlcNAc)_3$ and Ps-AFP1 was performed in order to verify the probable inter-molecular interactions. The Ps-AFP1 C-terminal segment seems to be mainly responsible for Ps-AFP1-$(GlcNAc)_3$ interactions (Fig. 6). This complexation is constructed by a hydrogen-bond net. The residues Ser^{28}, Ser^{33} and Arg^{37} interact through their side chains with hydrogen bonds, while the residues

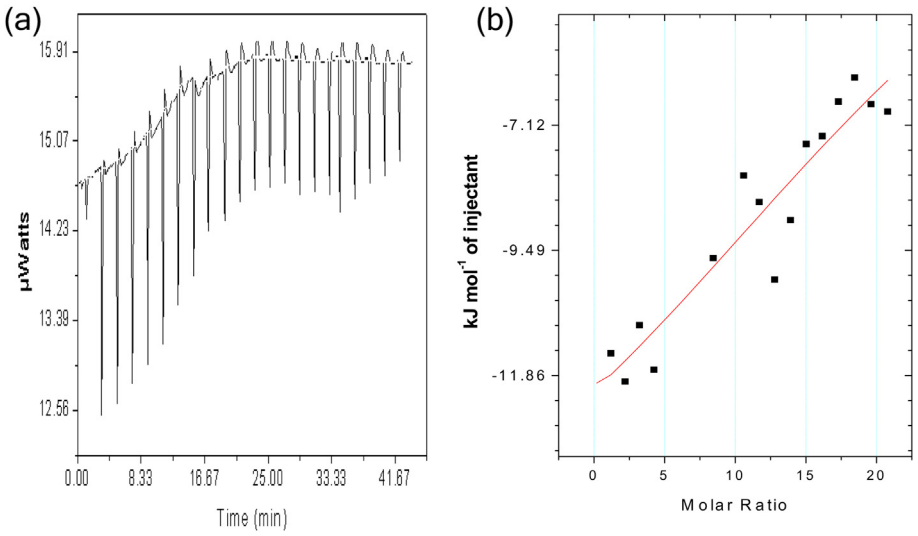

Fig. 4. ITC-based binding affinity measurement of Ps-AFP1 with $(GlcNAc)_3$. Binding thermogram and isotherm of Ps-AFP1 and $(GlcNAc)_3$ interaction are shown in figure as (a) and (b), respectively.

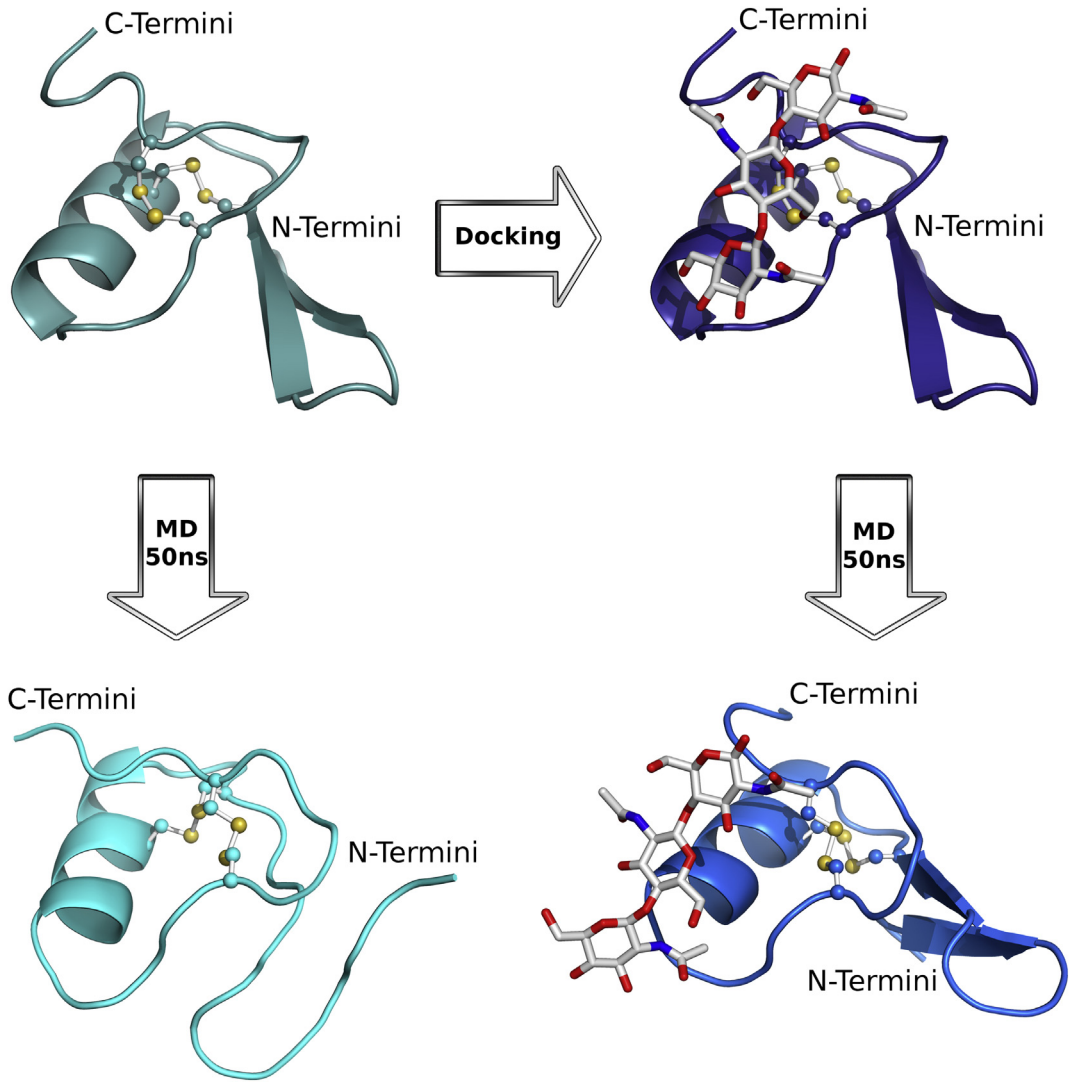

Fig. 5. Molecular model of Ps-AFP1 generated by QUARK and docking result of Ps-AFP1 and $(GlcNAc)_3$ (upper panels). Final structures after 50 ns of simulation (lower panels). Disulfide bonds are represented as ball and stick.

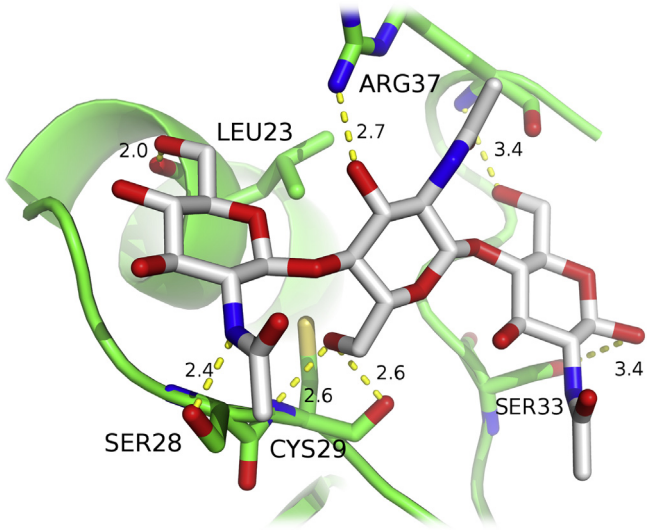

Fig. 6. Docking results of Ps-AFP1 and $(GlcNAc)_3$. The residues that contribute to hydrogen bonds are shown as sticks. Distances are measured in angstroms.

Leu^{23}, Cys^{29} and Arg^{37} interact through their main chain also by hydrogen bonds (Fig. 6).

In order to evaluate the structure prediction and the binding affinities between Ps-AFP1 and $(GlcNAc)_3$, two distinct molecular dynamics were performed. Firstly, the peptide simulation in water environment was performed, where a fold loss could be observed in the β-sheet (Fig. 5). In addition, the tertiary structure seemed to be unstable in water, since the backbone's RMSD variation throughout the simulation was very irregular and did not reach stabilization (Fig. 7A). Nevertheless, the simulation of the peptide-$(GlcNAc)_3$ complex showed the opposite situation. Interestingly, the complex seemed to be more stable than the free peptide, so that no losses of secondary structures were observed (Fig. 5), and the RMSD variation during the simulation was more constant (Fig. 7A), indicating that the $(GlcNAc)_3$ stabilized the Ps-AFP1 structure. This stabilization was also indicated by the RMSF, where virtually all residues were more stable when Ps-AFP1 was in complex with $(GlcNAc)_3$ (Fig. 7B).

3. Discussion

Plant seeds seem to be excellent targets for identification of novel antimicrobial peptides, and a number of AMPs have already

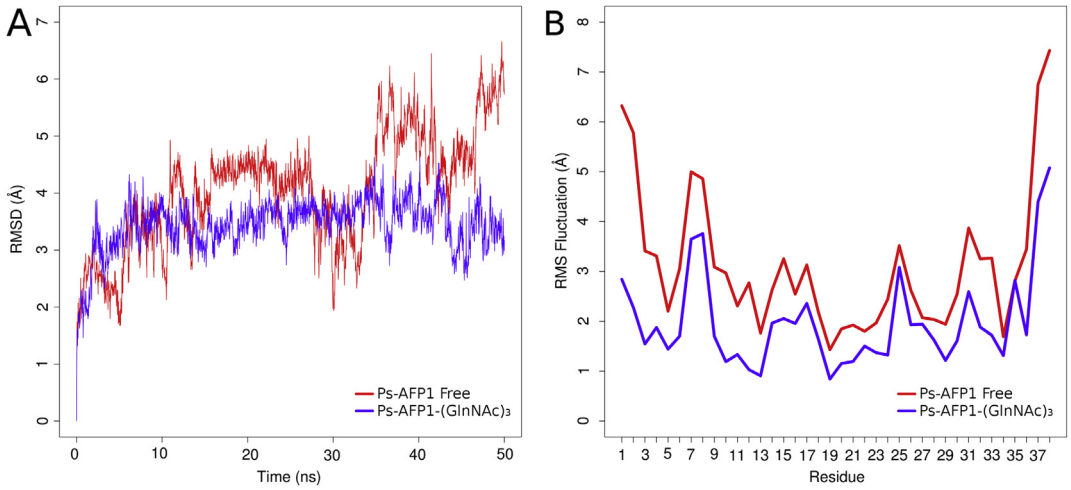

Fig. 7. Backbone RMSD (A) and RMS fluctuation (B) of Ps-AFP1 during 50 ns of simulation, the free peptide in red and the peptide-$(GlcNAc)_3$ in blue.

been identified as active against fungal and bacterial phytopathogens [29]. This report describes a novel peptide in the radicle of germinating *P. sativum* seeds, named Ps-AFP1. Ps-AFP1 is able to inhibit the germination of fungal spores and is probably involved in root defense in the first stages of plant development, since the radicle is the first soft tissue to emerge from germinating seeds.

Initially, the HPLC fractions from the *P. sativum* radicle's acidic extract were screened for antifungal activity. Among the HPLC fractions, one of them was found to exert strong antifungal activity (Fig. 1). Therefore, Ps-AFP1 was purified and sequenced, revealing a peptide with 38 amino acid residues, containing four cysteine residues, involved in two disulfide bonds. Ps-AFP1 showed a remarkable feature, being composed of seven arginine, six serine and six leucine residues, totaling half of peptide composition. Interestingly, neither homologs nor domains were found for Ps-AFP1 through PSI-BLAST and InterPro Scan, respectively. The similarities between Ps-AFP1 and the other cysteine-stabilized AMPs are restricted to the physicochemical properties, since a positive antimicrobial activity prediction was returned by CS-AMPPred. As Ps-AFP1's antifungal activity was known before its sequencing, we conducted antimicrobial activity prediction not to predict the activity itself, but in order to verify if Ps-AFP1's properties were similar to those of other cysteine-stabilized AMPs.

The absence of related sequences leads us to believe that Ps-AFP1 could belong to a novel AMP class, despite the fact that this novel class has only one member so far, Ps-AFP1 itself. In order to clarify this issue, *in silico* structural analyses were performed. Initially, threading algorithms were used to select the best template for comparative modeling; however, no significant templates were found. Thus, *ab initio* molecular modeling was performed. The prediction indicates that Ps-AFP1 belongs to the cysteine-stabilized AMP group. However, its disulfide bond pattern is distinct from the well-known AMP classes, as is its fold, composed of an α-helix and an antiparallel β-sheet with two β-strands. Ps-AFP1 was directly compared to all previously described plant AMP classes and especially to the plant defensins. Nevertheless, no match was obtained, and for this reason a novel class of plant AMPs was proposed and named the αβ-trumpet peptides. Defensins with the CSαβ motif are stabilized at least by three disulphide bonds, as observed for PsD1 [56], showing two characteristic motifs of CXC (present in a β-strand) and CXXXC (present in a α-helix) [2,9,12]. This specific pattern was not observed here. For this reason, a novel peptide fold, named αβ-trumpet, was here proposed, referring to the musical instrument, since the loop connecting the two β-strands would be the tuning slide and the α-helix would be the trumpet bell (Fig. S2). Continuing the analogy, it seems that the trumpet plays when phytopathogens attack the radicle, being involved in the first defense line of the germination process. Other classes of AMPs were also observed during the germination process, including defensins [9] and 2S albumins [29], which compose a chemical army (maybe a symphony) to protect the seedling from phytopathogenic attack.

The confocal microscopic images clearly revealed that Ps-AFP1 is mainly located on the fungal cell surface (Fig. 3), indicating that the target could be something extracellular, such as the cell membrane, the cell wall or even a cell receptor. However, scanning electron microscopy shows morphological modifications in fungal spores with deleterious effects on hyphal elongation (Fig. 2). Similarly, the peptide IWF4, which was purified from sugar-beet (*Beta vulgaris* L.) leaves, was able to inhibit the fungi's hyphal elongation and spore germination with their chitin binding properties [30]. Since the major spore-coating component is chitin, the proposed target for Ps-AFP1 was the fungal cell wall. In order to better understand the peptide target, an ITC experiment was performed. The ITC analyses showed that Ps-AFP1 was able to make a real interaction to $(GlcNAc)_3$ (Fig. 4). Therefore, molecular docking followed and molecular dynamics were performed to investigate the Ps-AFP1-$(GlcNAc)_3$ interactions. The simulations clearly indicate the need for $(GlcNAc)_3$ as a ligand to stabilize the structure of Ps-AFP1 (Figs. 5 and 7A). The complex was maintained during the whole simulation, indicating that it binds to chitin, as showed by ITC experiments. In this view, Ps-AFP1 can be classified as a lectin, since the definition of lectin is a peptide or protein that has at least one domain with ability to bind reversibly and non-enzymatically to a specific carbohydrate [5], which could be a mono- or oligosaccharide. In the case of Ps-AFP1 the carbohydrate seems to be $(GlcNAc)_3$. Lectins can be found in plants [5,22], animals [31], fungi [5,32] and bacteria [33], being observed at subcellular levels in membranes and cell secretions [34]. They are involved in numerous biological processes, including defense against pathogens, symbiosis and cell signaling [34]. Among pathogen defense functions, lectins can perform bactericidal [35], fungicidal [5,35] and antiviral activities [36]. In the case of Ps-AFP1, only antifungal activity is reported until now. The mechanism of action of Ps-AFP1 could be similar to the class of hevein-like peptides, where the peptide binds to the cell wall, inhibiting its elongation and leading the fungus to death [5].

In summary, a novel AMP class is proposed, the αβ-trumpet peptides, with a single member so far: the peptide Ps-AFP1. This peptide was isolated from *P. sativum* seeds during the germination

phase. It is probably involved in plant defense against fungi in the initial development stages, being extremely valuable for plant survival. The Ps-AFP1 mechanism of action seems to be related to chitin interactions, inhibiting fungal development. Additional studies are needed for a better functional and structural characterization of Ps-AFP1. Data here presented suggest that in the near future Ps-AFP could be used as a potent biotechnological tool in the control of novel antifungal agents.

4. Material and methods

4.1. Sample collection

P. sativum seeds were locally obtained. Seeds were left to germinate after overnight soaking in water. Radicles emerged from the seeds, reaching 2–3 mm in length after incubation for two days at room temperature. The radicles were sliced out and kept at −20 °C until further use.

4.2. Sample preparation

The radicles were frozen in liquid nitrogen and ground well with a pestle and mortar. The obtained radicle powder was homogenized with 0.5% aqueous acetic acid solution and incubated overnight in a rotary shaker with 120 rpm. The resulting acetic acid extracted solution was repeatedly centrifuged at 12,000 rpm and further filtered with 0.22 μM filter (Millipore, USA) before further purification process.

4.3. Peptide separation and purification

The extracted acetic acid solution was fractionated by reverse phase HPLC (Agilent 1100 series) with a ZORBAX 300-SB18 column (4.6 mm × 250 mm, particle size 5 μm), at a flow rate of 1 mL min^{-1}. The solvent was 0.1% aqueous TFA (A) and 80% acetonitrile containing 0.1% TFA (B). A step gradient of solvent B used to run the column was as follows: 0–60% for 0–45 min, 60–80% for 45–55 min and 80–100% for 55–60 min. All the solvents of HPLC grade were purchased from Spectrochem, India. The elution of adsorbed proteins was monitored at 215 nm. Collected fractions were concentrated by lyophilization and antifungal activity was screened as described above. The fraction showing antifungal activity was re-chromatographed in the same column and same conditions, but solvent B was used as 100% ACN with a gradient of 0–10% for 30 min, the eluted single peak was concentrated by lyophilization and further antifungal and analytical assays were performed. Peptide concentration was determined using the same RP-HPLC conditions and calibrated with bovine insulin (Sigma–Aldrich).

4.4. MALDI–TOF-MS analysis

The lyophilized mostly active peptide fraction was re-suspended in 80% (v/v) acetonitrile solution containing 0.1% (v/v) trifluoroacetic acid, and 4 μL of peptide solution was mixed with 4 μL of matrix (CHCA, 10 mg mL^{-1}). One microliter of this mixture solution was spotted onto the MALDI 100 well stainless steel sample plate and allowed to air-dry prior to the MALDI analysis. To obtain MALDI mass spectra, a Voyager time-of-flight mass spectrometer (Applied Biosystem, USA), equipped with 337 nm N_2 laser was used and operated in accelerating 20 kV voltage. The spectra were recorded in the positive ion linear mode. Reproducibility of the spectrum was checked several times from separately spotted samples.

4.5. Antifungal bioassays

Antifungal activity of purified peptide Ps-AFP1 was evaluated against *A. niger*, *Aspergillus terreus*, *F. solani*, *F. oxysporum*, *Pythium* sp., *C. gloeosporioides*, *Glomerella* sp. and *C. albicans* as earlier described [37]. Wells were filled with 10 μL of two-fold serial dilutions of the peptide and mixed with 90 μL half-strength potato-dextrose broth containing conidia or zoosporangia (~ 10^4 cells mL^{-1}). The inhibition of spore germination was evaluated by measuring the absorbance at 620 nm. Morphological changes were recorded using a light microscope. Antifungal activity was expressed by the peptide concentration causing a 50% inhibition of fungal growth (EC_{50}). Experiments were repeated three times.

In vitro growth kinetics of fungal strains (*C. albicans* and *C. gloeosporioides*) were determined following the protocol described by Mitchell et al. [38]. Fungal strains (10^3 CFU) were inoculated into 2 mL Sabouraud dextrose broth supplemented with different doses of Ps-AFP1 (1.0–12.0 μM), and further incubated at 30 °C with continuous shaking at 180 rpm. Two milliliters of mock-inoculated Sabouraud dextrose broth served as a negative control. The *in vitro* growth rates were measured at OD_{600} and using the conversion factor of 3 × 10^7 CFU mL^{-1} per 1 U OD_{600} [38]. Experiments were repeated thrice and data were presented as mean of triplicates ± S.E.

4.6. N-terminal amino acid sequencing

The peptide was run onto Tricine-SDS-PAGE, further transferred to PVDF membrane (Bio-Rad), stained with amido black (Sigma) for 2–3 min, marked and de-stained with repetitive washing with 50% methanol. The membrane was finally rinsed in Milli-Q water. The marked region of the membrane was cut and subjected to N-terminal sequencing. The N-terminal sequence was determined by automatic degradation in Procise 491 CLC protein sequencer (Applied Biosystems).

4.7. Circular dichroism analysis

The circular dichroism (CD) spectrum of the active fraction (Fr.3) was recorded at 37 °C using a Jasco J-815 spectropolarimeter equipped with a Jasco PTC-423 S Peltier temperature controller. The scanning rate was 50 nm min^{-1} with a response time of 2 s. The spectrum was recorded at standard sensitivity (100 mdeg) with a data-pitch of 0.5 nmin continuous mode. The scanning range was 245–180 nm and spectrum was the average of two consequent accumulations. The baseline was corrected by subtracting the corresponding buffer blank.

4.8. Radicle RNA isolation

Fresh radicle (200 mg) was put in a pre-chilled mortar and homogenized in liquid N2. Then an equal volume of saturated phenol and RNA extraction buffer (pre equilibrated at 85 °C) was added and mixed well, incubated at 85 °C for 10 min with vigorous shaking. Half volume of $CHCl_3$ was added to it and then mixed for 5 min. The upper aqueous layer was taken after centrifugation at 10,000 rpm for 10 min and RNA precipitated with 1/10th volume of 3 M sodium acetate (pH 5.2) and 2.5 volume of chilled ethanol at −70 °C overnight. RNA was pelleted by centrifugation at 8000 rpm for 20 min at 4 °C. The pellet was washed twice with chilled 70% alcohol, air-dried and dissolved in RNase-free water. The quality of RNA was checked by integrity of ribosomal RNA bands in agarose gel (1%) electrophoresis and quantified using UV-spectrophotometry. To remove any DNA contamination, the RNA

was treated with RNase-free DNase I (Boehringer Mannheim) in the presence of $MgCl_2$ (final conc. 10 mM) at 28 °C for 30 min.

4.9. 3′ RACE (rapid amplification of cDNA ends) and PCR amplification

For the 3′ RACE experiment, a poly (A) tail was synthesized using poly (A) polymerase at the 3′ ends (Invitrogen). The polymerization reaction was carried out with 5 μg of RNA in a final volume of 50 μL containing 50 mM Tris–HCl (pH 7.9), 10 mM $MgCl_2$, 2.5 mM $MnCl_2$, 50 mM NaCl, 250 μM ATP, 500 μg mL^{-1} BSA and 5 U poly (A) polymerase for 2 h at 37 °C. Polyadenylated RNA was purified by phenol–$CHCl_3$ extraction and ethanol precipitation overnight at −70 °C. Subsequently, 1st strand cDNA was synthesized using AOT (oligo dT adapter) primer at 48 °C for 1 h. PCR was carried out with polyadenylated cDNA as template using the 5′ gene-specific primer designed on the basis of N-terminal sequence of the peptide and 3′ RACE-AMP primer (provided in kit) that annealed to the poly (A) tail. PCR was done under the following thermal profile: initial denaturation at 94 °C for 4 min, followed by 30 cycles of 94 °C/30°s, 55 °C/30 s, 72 °C/30 s and a final extension at 72 °C for 5 min with Taq DNA polymerase (Roche). The 3′ RACE PCR product was resolved in 1.0% agarose gel, eluted using quick gel extraction kit (QIAGEN) and cloned into pCR2.1-TOPO vector. Recombinant plasmid pCR2.1-TOPO10/RACE PCR product was sequenced using M13 forward and reverse primer with Bigdye terminator kit (ABI).

4.10. Microscopy and spore germination inhibition

Spore germination inhibition assay was performed following Nolde et al. [23]. Spore suspension ($\sim 10^6$ spores mL^{-1}, 385 μL per well) of *Glomerella* sp. was placed in an 8-well Lab-Tek chambered cover glass (Nalge Nunc International), and the spores became attached to the chamber bottom. Spores were incubated with a fixed peptide concentration that corresponded to their 50% (EC_{50}) inhibitory effect of fungal growth. 1× PBS control was used and incubation monitored every 2 h interval up to 6 h. The treated spores were visualized in phase contrast microscope (Olympus 1X51) and images were captured at 1000× magnification.

4.11. Preparation of fluorescein isothiocyanate (FITC) conjugated Ps-AFP1

Both FITC and Ps-AFP1 were dissolved in 100 μL of DMSO to make a final concentration of 10 mg mL^{-1}, and 8 μM, respectively. Both the solutions were mixed together and incubated in the dark at room temperature for 4 h. Further, 1 M ethanolamine was added to inactivate the residual FITC. Then FITC-conjugated Ps-AFP1 was purified by being sequentially chromatographed on a gel-filtration column following the protocol described by Ref. [39].

4.12. Confocal microscopy

Candida cells were grown for 18 h in potato-dextrose broth. Cells were collected and washed gently with PBS (1×) buffer. The cell suspension (100 μL) was prepared in PBS containing 5×10^4 cells mL^{-1}. Cells were treated with 2 drops of 0.1% calcofluor white M2R (CFW) for 2 min in the dark and further treated with FITC-conjugated Ps-AFP1 for another 5 and 10 min respectively. Cells were then visualized by confocal microscopy using a Leica TCS SP2 confocal microscope (Leica). FITC and CFW were excited using a 488 and 355-nm laser, respectively. Images were captured using confocal LCS 3D software (Leica) and processed with the same manufacturer's software.

4.13. Isothermal titration calorimetry assays

In order to measure the binding affinity of *N*-acetyl-D-glucosamine (GlcNAc) with peptide, Ps-AFP1, isothermal titration calorimetry (ITC) was performed using iTC200 Systems equipment (GE Healthcare, USA) coupled with non-reactive Hastelloy® cells for chemical resistance. All pure samples were dissolved against phosphate buffer (pH 7.5). Ten μM Ps-AFP1 and 1 μM GlcNAc were prepared to be used as the ligand and macromolecules in ITC experiments. All solutions were degassed right before the experimental runs in same conditions at 25 °C and at 180-s intervals utilizing a stir speed of 310 rpm. Blank ITC experiments were done to correct heat of dilution effects. Origin 7.0 (OriginLab Corp., MA) was used to analyze the ITC data to determine the binding constant (K) and enthalpy of binding (ΔH) directly from the binding thermograms.

4.14. Sequence analysis and molecular modeling

The similarity search was done by using PSI-BLAST [40] in the NCBI's non-redundant protein database. Then, domain identification was done by using InterPro Scan [41]. Antimicrobial activity prediction was done by using the polynomial model of CS-AMPPred [42,43]. The QUARK *ab initio* modeling server [44] was used for generating the three-dimensional structure of Ps-AFP1, since no significant templates for comparative modeling were found through the LOMETS server [45]. Subsequently, the Swiss PDB Viewer [46] was used for adjusting the distances between the sulfur atoms to 2 Å, followed by an energy minimization with 2000 steps of steepest descent using the GROMOS96 implementation of Swiss PDB Viewer [46]. The minimized model was evaluated through PROSA II [47] and PROCHECK [48]. PROCHECK checks the stereochemical quality of a protein structure, through the Ramachandran plot, where reliable models are expected to have more than 90% of amino acid residues in most favored and additional allowed regions. PROCHECK also gives the G-factor, a measurement of how unusual the model is, where values below −0.5 are unusual, while PROSA II indicates the fold quality.

4.15. Molecular docking and dynamics

The complex between Ps-AFP1 and *N*,*N*,*N*-triacetylchitotriose ($(GlcNAc)_3$) was constructed through Hex 6.1 [49]. The coordinates of $(GlcNAc)_3$ were obtained from the structure of hevein-32 (PDB ID: 1T0W) [50]. Docking experiments were performed considering shape and electrostatics of each molecule without any docking post processing. The resulting complexes were clustered, using RMS cut-off of 3 Å. The cluster with highest affinity was selected as the preferable binding mode. The GROMACS package (version 4.5) [51] was used for performing the molecular dynamics simulations (MD). Two distinct simulations were done, one with the free peptide and another with the peptide-$(GlcNAc)_3$ complex. The molecular models were immersed in a cubic water box, with a distance of 0.5 nm from the edge of each box. Water molecules were represented by the single point charge water model [52]. Chlorine ions were added to the system in order to neutralize the system's charge. Fifty thousand steps of steepest descent were performed to minimize the system. Following that, the molecular dynamics integrator was used for pressure and temperature normalization (100 ps each) by using the velocity rescaling thermostat (NVT ensemble) and the Parrinello-Rahman barostat (NPT ensemble), respectively. Then, the system with minimized energy and normalized pressure and temperature was simulated for 50 ns. The simulations were carried out *in silico* at 300 K and 1 bar. The geometry of water molecules was constrained by using the SETTLE algorithm [53]; and all atom bond lengths were linked by using the

LINCS algorithm [54]. The electrostatic corrections were made by Particle Mesh Ewald algorithm [55], with a cut-off radius of 1.4 nm; the same cut-off radius was also used for van der Waals interactions. The MD simulations were analyzed by means of root-mean-square deviation (RMSD) and root-mean-square fluctuation (RMSF).

Acknowledgments

This work received grants from CNPq, CAPES and FAPDF.

Appendix A. Supplementary data

Supplementary data related to this article can be found at http://dx.doi.org/10.1016/j.biochi.2013.06.027.

References

[1] P.B. Pelegrini, E.F. Noronha, M.A.R. Muniz, I.M. Vasconcelos, M.D. Chiarello, et al., An antifungal peptide from passion fruit (*Passiflora edulis*) seeds with similarities to 2S albumin proteins, Biochim. Biophys. Acta 1764 (6) (2006) 1141–1146.
[2] E.S. Cândido, W.F. Porto, D.S. Amaro, J.C. Viana, S.C. Dias, O.L. Franco, Structural and functional insights into plant bactericidal peptides, in: A. Méndez-Vilas (Ed.), Science Against Microbial Pathogens: Communicating Current Research and Technological Advances, 2011, pp. 951–960.
[3] F. García-Olmedo, A.M. Fernández, J.M. Alamillo, P.R. Palenzuela, Plant defense peptides, Pep. Sci. 47 (6) (1998) 479–491.
[4] K.A.T. Silverstein, W.A. Moskal, H.C. Wu, B.A. Underwood, M.A. Graham, et al., Small cysteine-rich peptides resembling antimicrobial peptides have been under-predicted in plants, Plant J. 51 (2) (2007) 262–280.
[5] W.F. Porto, V.A. Souza, D.O. Nolasco, O.L. Franco, In silico identification of novel hevein-like peptide precursors, Peptides 38 (2012) 127–136.
[6] P.B. Pelegrini, A.M. Murad, L.P. Silva, R.C. Dos Santos, F.T. Costa, et al., Identification of a novel storage glycine-rich peptide from guava (*Psidium guajava*) seeds with activity against Gram-negative bacteria, Peptides 29 (8) (2006) 1271–1279.
[7] S.M. Mandal, L. Migliolo, S. Das, M. Mandal, O.L. Franco, T.K. Hazra, Identification and characterization of a bactericidal and proapoptotic peptide from *Cycas revoluta* seeds with DNA binding properties, J. Cell. Biochem. 133 (2012) 184–193.
[8] P.B. Pelegrini, L.R. Farias, A.C. Saude, F.T. Costa, C. Bloch Jr., et al., A novel antimicrobial peptide from *Crotalaria pallida* seeds with activity against human and phytopathogens, Curr. Microbiol. 59 (4) (2009) 400–404.
[9] O.L. Franco, A.M. Murad, J.R. Leite, P.A. Mendes, M.V. Prates, C. Bloch Jr., Identification of a cowpea gamma-thionin with bactericidal activity, FEBS J. 273 (15) (2006) 3489–3497.
[10] K.A. Brogden, Antimicrobial peptides: pore formers or metabolic inhibitors in bacteria? Nat. Rev. Microbiol. 3 (3) (2005) 238–250.
[11] A.M. McManus, K.J. Nielsen, J.P. Marcus, S.J. Harrison, J.L. Green, et al., MiAMP1, a novel protein from *Macadamia integrifolia* adopts a Greek key beta-barrel fold unique amongst plant antimicrobial proteins, J. Mol. Biol. 293 (3) (1999) 629–638.
[12] O.L. Franco, Peptide promiscuity: an evolutionary concept for plant defense, FEBS Lett. 585 (7) (2011) 995–1000.
[13] L.S. Tavares, J.V. Rettore, R.M. Freitas, W.F. Porto, A.P. Duque, et al., Antimicrobial activity of recombinant Pg-AMP1, a glycine-rich peptide from guava seeds, Peptides 37 (2) (2012) 294–300.
[14] S.M. Mandal, S. Dey, M. Mandal, S. Sarkar, S. Maria-Neto, O.L. Franco, Identification and structural insights of three novel antimicrobial peptides isolated from green coconut water, Peptides 30 (4) (2009) 633–637;
G.H. Gao, W. Liu, J.X. Dai, J.F. Wang, Z. Hu, et al., Solution structure of PAFP-S: a new knottin-type antifungal peptide from the seeds of *Phytolacca americana*, Biochemistry 40 (37) (2001) 10973–10978.
[15] O.N. Silva, W.F. Porto, L. Migliolo, S.M. Mandal, D.G. Gomes, et al., Cn-AMP-1: a new promiscuous peptide with potential for microbial infections treatment, Biopolymers 98 (4) (2012) 322–331.
[16] M. Fujimura, M. Ideguchi, Y. Minami, K. Watanabe, K. Tadera, Tu-AMP 1 and Tu-AMP 2, from bulbs of tulip (*Tulipa gesneriana* L.), Biosci. Biotechnol. Biochem. 68 (3) (2004) 571–577.
[17] S. Romagnoli, R. Ugolini, F. Fogolari, G. Schaller, K. Urech, M. Giannattasio, et al., NMR structural determination of viscotoxin A3 from *Viscum album* L, Biochem. J. 350 (2000) 569–577.
[18] K.C. Chen, C.Y. Lin, M.C. Chung, C.C. Kuan, H.Y. Sung, S.C.S. Tsou, et al., Cloning and characterization of a cDNA encoding an antimicrobial protein from mung bean seeds, Bot. Bull. Acad. Sin. 43 (2002) 251–259.
[19] N.Y. Yount, M.R. Yeaman, Multidimensional signatures in antimicrobial peptides, Proc. Natl. Acad. Sci. U.S.A. 101 (19) (2004) 7363–7368.
[20] M.F. Pinto, I.C. Fensterseifer, L. Migliolo, D.A. Sousa, G. de Capdeville, J.W. Arboleda-Valencia, et al., Identification and structural characterization of novel cyclotide with activity against an insect pest of sugar cane, J. Biol. Chem. 287 (2012) 134–147.
[21] M.F.S. Pinto, R.G. Almeida, W.F. Porto, I.C.M. Fensterseifer, L.A. Lima, S.C. Dias, et al., Cyclotides: from gene structure to promiscuous multifunctionality, J. Evid. Based Complementary Altern. Med. 17 (2012) 40–53.
[22] W.F. Broekaert, W. Mariën, F.R. Terras, M.F. De Bolle, P. Proost, J. Van Damme, et al., Antimicrobial peptides from *Amaranthus caudatus* seeds with sequence homology to the cysteine/glycine-rich domain of chitin-binding proteins, Biochemistry 31 (17) (1992) 4308–4314.
[23] S.B. Nolde, A.A. Vassilevski, E.A. Rogozhin, N.A. Barinov, T.A. Balashova, O.V. Samsonova, et al., Disulfide-stabilized helical hairpin structure and activity of a novel antifungal peptide EcAMP1 from seeds of barnyard grass (*Echinochloa crus-galli*), J. Biol. Chem. 286 (28) (2011) 25145–25153.
[24] P.B. Oparin, K.S. Mineev, Y.E. Dunaevsky, A.S. Arseniev, M.A. Belozersky, E.V. Grishin, et al., Buckwheat trypsin inhibitor with helical hairpin structure belongs to a new family of plant defence peptides, Biochem. J. 446 (2012) 69–77.
[25] A. Segura, M. Moreno, F. Madueño, A. Molina, F. García-Olmedo, Snakin-1, a peptide from potato that is active against plant pathogens, Mol. Plant Microbe Interact. 12 (1999) 16–23.
[26] M. Berrocal-Lobo, A. Segura, M. Moreno, G. López, F. García-Olmedo, A. Molina, Sankin-2, an antimicrobial peptide from potato whose gene is locally induced by wounding and responds to pathogen infection, Plant Physiol. 128 (3) (2002) 951–961.
[27] W.F. Porto, O.L. Franco, Theoretical structural insights into the snakin/GASA family, Peptides 44 (2013) 163–167.
[28] Z.K. Punja, Genetic engineering of plants to enhance resistance to fungal pathogens – a review of progress and future prospects, Can. J. Plant Pathol. 23 (2001) 216–235.
[29] E.S. Cândido, M.F. Pinto, P.B. Pelegrini, T.B. Lima, O.N. Silva, et al., Plant storage proteins with antimicrobial activity: novel insights into plant defense mechanisms, FASEB J. 25 (10) (2011) 3290–3305.
[30] K.K. Nielsen, J.E. Nielsen, S.M. Madrid, J.D. Mikkelsen, Characterization of a new antifungal chitin-binding peptide from sugar beet leaves, Plant Physiol. 113 (1997) 83–91.
[31] D.S. Medeiros, T.L. Medeiros, J.K. Ribeiro, N.K. Monteiro, L. Migliolo, et al., A lactose specific lectin from the sponge *Cinachyrella apion*: purification, characterization, N-terminal sequences alignment and agglutinating activity on *Leishmania promastigotes*, Comp. Biochem. Physiol. B Biochem. Mol. Biol. 155 (3) (2010) 211–216.
[32] J. Inbar, I. Chet, A newly isolated lectin from the plant pathogenic fungus *Sclerotium rolfsii*: purification, characterization and role in mycoparasitism, Microbiology 140 (Pt. 3) (1994) 651–657.
[33] S. Kolbe, S. Fischer, A. Becirevic, P. Hinz, H. Schrempf, The *Streptomyces reticuli* α-chitin-binding protein CHB2 and its gene, Microbiology 144 (Pt. 5) (1998) 1291–1297.
[34] P.L. De Hoff, L.M. Brill, A.M. Hirsch, Plant lectins: the ties that bind in root symbiosis and plant defense, Mol. Genet. Genomics 282 (2009) 1–15.
[35] J.C. Martins, D. Maes, R. Loris, H.A. Pepermans, L. Wyns, et al., H NMR study of the solution structure of Ac-AMP2, a sugar binding antimicrobial protein isolated from *Amaranthus caudatus*, J. Mol. Biol. 258 (2) (1996) 322–333.
[36] Y. Luo, X. Xu, J. Liu, J. Li, Y. Sun, et al., A novel mannose-binding tuber lectin from *Typhonium divaricatum* (L.) Decne (family Araceae) with antiviral activity against HSV-II and anti-proliferative effect on human cancer cell lines, J. Biochem. Mol. Biol. 40 (3) (2007) 358–367.
[37] W.F. Broekaert, F.R.G. Terras, B.P.A. Cammue, J. Vanderleyden, An automated quantitative assay for fungal growth inhibition, FEMS Microbiol. Lett. 69 (1990) 55–59.
[38] B.M. Mitchell, T.G. Wu, B.E. Jackson, K.R. Wilhelmus, *Candida albicans* strain-dependent virulence and Rim13p-mediated filamentation in experimental keratomycosis, Invest. Ophthalmol. Vis. Sci. 48 (2007) 774–780.
[39] D.G. Lee, K.S. Hahm, Y. Park, H.Y. Kim, W. Lee, et al., Functional and structural characteristics of anticancer peptide Pep27 analogues, Cancer Cell Int. 5 (2005) 11.
[40] S.F. Altschul, T.L. Madden, A.A. Schäffer, J. Zhang, Z. Zhang, et al., Gapped BLAST and PSI-BLAST: a new generation of protein database search programs, Nucleic Acids Res. 25 (17) (1997) 3389–3402.
[41] E. Quevillon, V. Silventoinen, S. Pillai, N. Harte, N. Mulder, et al., InterProScan: protein domains identifier, Nucleic Acids Res. 33 (2005) 116–120.
[42] W.F. Porto, F.C. Fernandes, O.L. Franco, An SVM model based on physicochemical properties to predict antimicrobial activity from protein sequences with cysteine knot motifs, Lect. Notes Comput. Sci. 6268 (2010) 59–62.
[43] W.F. Porto, A.S. Pires, O.L. Franco, CS-AMPPred: an updated SVM model for antimicrobial activity prediction in cysteine-stabilized peptides, PLoS ONE 7 (12) (2012) e51444.
[44] D. Xu, Y. Zhang, Ab initio protein structure assembly using continuous structure fragments and optimized knowledge-based force field, Proteins 80 (2012) 1715–1735.
[45] S. Wu, Y. Zhang, LOMETS: a local meta-threading-server for protein structure prediction, Nucleic Acids Res. 35 (10) (2007) 3375–3382.
[46] N. Guex, M.C. Peitsch, SWISS-MODEL and the Swiss-PdbViewer: an environment for comparative protein modeling, Electrophoresis 18 (15) (1997) 2714–2723.
[47] M. Wiederstein, M.J. Sippl, ProSA-web: interactive web service for the recognition of errors in three-dimensional structures of proteins, Nucleic Acids Res. 35 (2007) 407–410.
[48] R.A. Laskowski, M.W. Macartur, D.S. Moss, J.M. Thornton, PROCHECK: a program to check the stereochemical quality of protein structures, J. Appl. Cryst. 26 (1993) 283–291.

[49] D.W. Ritchie, V. Venkatraman, Ultra-fast FFT protein docking on graphics processors, Bioinformatics 26 (19) (2010) 2398–2405.
[50] N. Aboitiz, M. Vila-Perelló, P. Groves, J.L. Asensio, D. Andreu, et al., NMR and modeling studies of protein–carbohydrate interactions: synthesis, three-dimensional structure, and recognition properties of a minimum hevein domain with binding affinity for chitooligosaccharides, Chembiochem 5 (9) (2004) 1245–1255.
[51] B. Hess, C. Kutzner, D. van der Spoel, E. Lindahl, GROMACS 4: algorithms for highly efficient, load-balanced, and scalable molecular simulation, J. Chem. Theory Comput. 4 (2008) 435–447.
[52] H.J.C. Berendsen, J.P.M. Postma, W.F. van Gunsteren, J. Hermans, Interaction models for water in relation to protein hydration, in: B. Pullman (Ed.), Intermolecular Force (1981), pp. 331–342.
[53] S. Miyamoto, P.A. Kollman, SETTLE. An analytical version of the SHAKE and RATTLE algorithm for rigid water models, J. Comput. Chem. 13 (8) (1992) 2134–2144.
[54] B. Hess, H. Bekker, H.J.C. Berendsen, J.G.E.M. Fraaije, LINCS. A linear constant solver for molecular simulations, J. Comput. Chem. 18 (12) (1997) 1463–1472.
[55] T. Darden, D. York, L. Pedersen, Particle mesh Ewald: an n long(n) method for Ewald sums in large systems, J. Chem. Phys. 98 (1993) 10089–10092.
[56] L.N. de Medeiros, R. Angeli, C.G. Sarzedas, F. Barreto-Bergter, A.P. Valente, E. Kurtenbach, F.C. Almeida, Backbone dynamics of the antifungal Psd1 pea defensin and its correlation with membrane interaction by NMR spectroscopy, Biochim. Biophys. Acta 1798 (2010) 105–113.